Editors' Suggestion

Large phosphorene in-plane contraction induced by interlayer interactions in graphene-phosphorene heterostructures

Benoit Van Troeye,* Aurélien Lherbier, Jean-Christophe Charlier, and Xavier Gonze
Institute of Condensed Matter and Nanosciences, Université catholique de Louvain, Chemin des étoiles 8, B-1348 Louvain-la-Neuve, Belgium

(Received 23 January 2018; published 10 July 2018)

Intralayer deformation in van der Waals (vdW) heterostructures is generally assumed to be negligible due to the weak nature of the interactions between the layers, especially when the interfaces are found incoherent. In the present work, graphene-phosphorene vdW heterostructures are investigated with the density functional theory (DFT). The challenge of treating a nearly incommensurate (very large) supercell in DFT is bypassed by considering different energetic quantities in the grand canonical ensemble, alternative to the formation energy, in order to take into account the mismatch elastic contribution of the different layers. In the investigated heterostructures, it is found that phosphorene contracts by ∼4% in the armchair direction when compared to its free-standing form. This large contraction leads to important changes in terms of electronic properties, with the direct electronic optical transition of phosphorene becoming indirect in specific vdW heterostructures. More generally, such a contraction indicates strong substrate effects in supported or encapsulated phosphorene—neglected hitherto—and paves the way to substrate-controlled stresstronic in such 2D crystal. In addition, the stability of these vdW heterostructures is investigated as a function of the rotation angle between the layers and as a function of the stacking composition. The alignment of the specific crystalline directions of graphene and phosphorene is found energetically favored. In parallel, several models based on DFT-estimated quantities are presented; they allow notably a better understanding of the global mutual accommodation of 2D materials in their corresponding interfaces, that is predicted to be non-negligible even in the case of incommensurate interfaces.

DOI: 10.1103/PhysRevMaterials.2.074001

I. INTRODUCTION

While the range of properties accessible by 2D materials is already quite broad [1], the construction of vdW heterostructures [1,2], obtained by stacking different 2D materials on top of the others, enables even more tunability with the addition of the "out-of-plane" building freedom. In such vdW heterostructures, the constituent layers are bound to the other ones by weak dispersive forces [3], which results in strongly-anisotropic properties, desirable, e.g., for electro-optic [4–6] or battery applications [7,8]. For the latter, nanocomposites based on alternating multilayers of graphene and phosphorene—a recently-discovered 2D material [9,10]—have demonstrated to outperform graphite as anode for sodium-ion battery in terms of specific capacity and cyclability [7]. However, understanding and predicting the phase formed by such vdW heterostructures, with the underlying questions of interface coherency [11] and commensurability, is still a hot topic, both from experimental and theoretical points of view.

Recently, an exactly-matched coherent graphene/h-BN vdW heterostructure has been grown recently by molecular beam epitaxy [12]. However, such a heterostructure has more generally been constructed using the pick-and-lift technique [1], and then reported either as a mesoscopic commensurate (semicoherent) structure [13–15] or an incommensurate (incoherent) one [13], depending on the rotation angle between the layers. In the semicoherent case, areas where graphene is exactly commensurate with h-BN [13] are separated by Frenkel-Kontorova domain walls where the accumulated strain is released. This leads to regions of preferential and nonpreferential stackings, which induces local buckling (corrugation) [16]. Such surface reconstruction has also been reported for $MoSe_2/WSe_2$ vdW heterostructure [17], or for silicene grown on MoS_2 [18]. Even in the case where the lattice mismatch is too large to observe a coherent interface, it is found that the alignment of common crystalline directions is more favorable, like for MoS_2 grown on graphene [19] or for germanene grown on MoS_2 [20]. Although the alignment of crystalline directions is reported as more favorable, other orientations can also be observed experimentally in some cases [19,21–23].

DFT [24] could bring valuable information on this question of interlayer coherence and the underlying question of commensurability/incommensurability of the phase. Unfortunately, the number of atoms reported experimentally for the primitive cell of semicoherent vdW heterostructures (i.e., thousands of atoms for graphene/h-BN) limits strongly its use. This problem has been generally tackled by the use of small unit cells associated with large deformations of the involved layers [25], or by the use of rotation angles that limit the intralayer deformations and the number of atoms to be considered [26,27]. The importance of the errors made by using these approximations is generally not investigated, since usual DFT codes are unfortunately unable to do so. One has to move to linear-scaling algorithms [28–31] or molecular dynamics simulations [32] to overcome this difficulty. Still,

*benoit.vantroeye@uclouvain.be

exploring the whole space of degrees of freedom (rotation angle and translation between the layers, as well as intralayer deformations) is an incredibly challenging task [30], even for these approaches, and generally goes beyond the precision of the technique.

Furthermore, even in the case of relatively small commensurate structures, the existing DFT computations do not consider consistently the relaxation of the unit cells and atomic positions. Focusing on the graphene-phosphorene systems, the phosphorene lattice has been either fixed to its free-standing form [25], with graphene taking thus the ∼7% deformation along the armchair direction, or the strain was arithmetically distributed between graphene and phosphorene [33,34]. Thanks to our systematic analyses of the intralayer degrees of freedom, we clarify the situation and show that it is in fact phosphorene that takes most of the deformation in graphene-phosphorene vdW heterostructures.

In the present paper, we investigate the properties of graphene-phosphorene vdW heterostructures as a function of their composition and stacking arrangements, in view of their application as anode in sodium-ion battery [7]. Thanks to DFT, we explore the energetics and structural properties of a series of small and medium unit cells, but also extract more transferable thermodynamic quantities and perform additional analyses based on a simple energy model, in order to alleviate to a large extent our DFT computational limitations.

The graphene-phosphorene vdW heterostructures studied in this paper consist of periodically-repeated out-of-plane few-layers-thick graphene and phosphorene domains, bound to another by weak dispersive forces. A special emphasis focuses on scanning both the rotational-angle and the intralayer-deformation degrees of freedom. For the first one, we investigate different commensurate structures and compare their energies with respect to different definitions of chemical potentials. The errors made by working with commensurate structures on energetics, can be greatly reduced by comparing the vdW-heterostructures to strained graphite and black phosphorus with the corresponding definitions of modified thermodynamical quantities. Thanks to these definitions, we are able to remove the spurious elastic strain induced by working with commensurate structures. Furthermore, we find that the most favorable angular configuration corresponds to the alignment of the crystalline directions of graphene and phosphorene (i.e., zigzag on zigzag and armchair on armchair). When such an aligned angular configuration is realized, all stacking and composition arrangements are found nearly equivalent in energy, indicating only very small energy penalty to form the graphene-phoshorene vdW interface compared to graphene-graphene and phosphorene-phosphorene vdW interfaces.

Concerning now the intralayer deformation, a qualitative model based on *ab initio* computed quantities and on the estimation of vdW energy thanks to Grimme's DFT-D3 method [35] has been developed. This model is validated on the phosphorene/black phosphorus system, where it allows us to understand the compression of the phosphorene armchair lattice parameter from the monolayer to the bulk, as observed for example in Ref. [31]. When applied to the graphene-phosphorene vdW heterostructures, this model reveals that the phosphorene layers compress quite significantly (∼4%) in the armchair direction in order to accommodate to the graphene lattice, and that even without considering coherency. This contraction leads to important modifications in the electronic band structures of the graphene-phosphorene vdW heterostructure when compared to the ones of isolated monolayers (and corresponding multilayers), turning the direct electronic transition of phosphorene into an indirect one.

This paper is organized as follows: First, in Sec. II, the computational details are presented, including convergence parameters, functional, and analysis of the building blocks (graphene and phosphorene) used to construct the vdW heterostructures. We also detail the methodology followed to build them. Second, in Sec. III, the different commensurate vdW heterostructures are characterized and their stabilities as functions of the rotation angle between the layers, composition, and stacking arrangements are discussed. In Sec. IV, a structural model, whose purpose is to investigate the intralayer-deformation degrees of freedom, is proposed, its validity verified on graphite and black phosphorus, and then applied to the specific case of the graphene-phosphorene vdW heterostructures. Finally, in Sec. V, the electronic properties of the graphene-phosphorene vdW heterostructures are presented and discussed. The Supplemental Material [36] includes additional discussions on graphite and black phosphorus, as well as additional figures, not presented in the main paper for sake of readability.

II. METHODOLOGY & BUILDING BLOCKS

All computations are performed using the ABINIT software [37–39]. The exchange-correlation energy is approximated using the GGA-PBE functional [40], corrected by Grimme's DFT-D3 for the long-range e^--e^- correlation [35,41]. For the sake of brevity, this combination of exchange-correlation and dispersion corrections will be denoted as PBE-D3 in the following. The cutoff radius for the coordination number, required for the dispersion corrections, is set to 105 Å, and only pairs contributing for more than 10^{-12} Ha are taken into account. Calculations are based on plane-waves and ONCVPSP norm-conserving pseudopotentials [42] from the PseudoDojo project [43] thus including multiple angular projectors. A plane-wave energy cutoff of 42 Ha and a $18 \times 18 \times 1$ Monkhorst-Pack wave-vector grid [44] are found sufficient for convergences of the ground-state properties of graphene and phosphorene building blocks. The in-plane wave-vector mesh is then adapted accordingly to the size of the supercell used to build the vdW heterostructures. An eight wave-vector out-of-plane sampling is used for their bulk counterparts (bernal graphite, black phosphorus, and the graphene-phosphorene vdW heterostructures). A Gaussian smearing of 0.01 Ha is applied for the occupation of states [45]. For the computation of isolated monolayers, cells with a 30 Bohr out-of-plane lattice vector are used.

In the prevision of the incoming analyses, we introduce the notion of cohesion energy that corresponds to the energy that

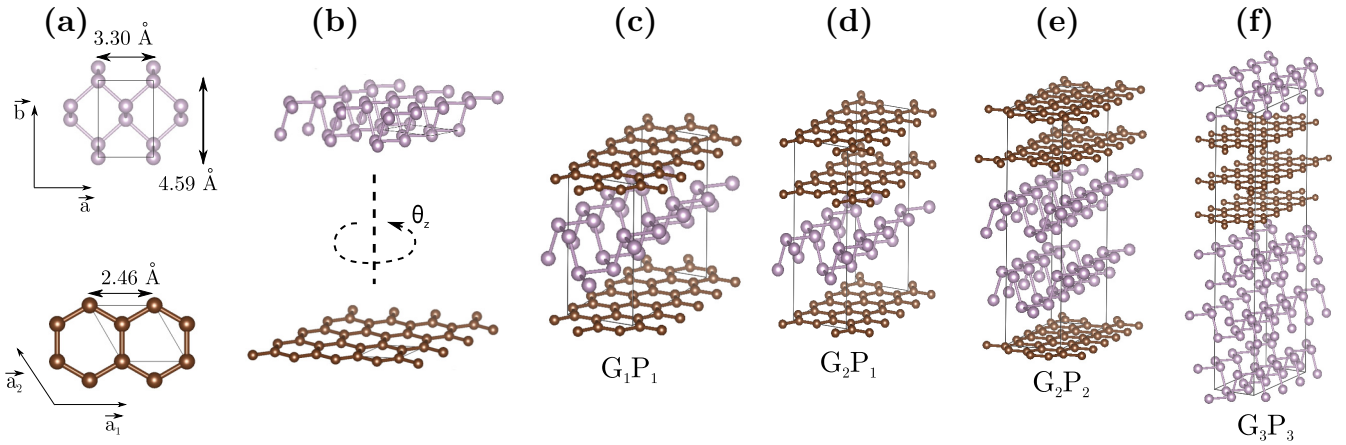

FIG. 1. Schematic construction and representation of the graphene-phosphorene vdW heterostructures studied in this paper. (a) Top view of the primitive cells of graphene and phosphorene, the two constituent building blocks of the heterostructure. (b) Superlattices of graphene and phosphorene are built and superposed for a given zigzag rotation angle θ_z between the layers. For that given angle, commensurate structures can be found with a corresponding strain tensor. From these commensurates, periodic graphene-phosphorene vdW heterostructures are constructed with different composition stackings as illustrated in (c)–(f). These structures are denoted G_iP_j where i and j correspond to the number of adjacent layers of graphene and phosphorene, respectively.

binds the layers together in a layered material:

$$E_{\text{coh}} = \frac{E_{\text{bulk}}}{N_{\text{bulk}}} - \frac{E_{\text{mono}}}{N_{\text{mono}}}, \tag{1}$$

where E_{bulk} and E_{mono} are the total energies of the bulk layered material and of the isolated layer (monolayer), respectively, while N_{bulk} and N_{mono} correspond to their respective number of atoms. In addition, the interlayer distance d_{int} is defined as the distance between the top of a layer and the bottom of the adjacent one.

The accuracy with respect to experiments [46–49], other DFT methods [50–53], and diffusion Monte Carlo (DMC) [52] of the combination of exchange-correlation, pseudopotentials, and dispersion corrections used in this paper is discussed in the Supplemental Material for graphite and black phosphorus. Both the ground-state and elastic properties (computed using the density functional perturbation theory (DFPT) [54–57]) are compared, specifically in Table S1. From this comparison, we point out that PBE-D3 yields in fact both reasonable lattice parameters and cohesive energies both in the case of graphite and black phosphorus, while concerning the predicted elastic constants, no conclusive remarks can be drawn on their accuracy from the available experimental and theoretical results [49,50,58,59].

In order to build the vdW heterostructures, we start from the (isolated monolayer) graphene and phosphorene primitive cells [see Fig. 1(a)] and their predicted lattice parameters as reported in Table I alongside with other theoretical results obtained with other dispersion corrections [9,31]. The intrinsic thickness of phosphorene is also reported in this table. Note that the armchair lattice parameter of phosphorene is larger (∼4%) than its counterpart in black phosphorus (see Supplemental Material). This expansion has also been observed using optB88-vdW [31] (2.5%) or PBE corrected by Grimme's DFT-D2 [60] (4%), while DMC predicts on the contrary a contraction of 2% from the bulk to the monolayer [52]. In fact, as discussed in the following (see Sec. IV), this effect results already from a tradeoff between interlayer interactions—including vdW ones—and elastic deformation. In the same table, the elastic constants per area unit $\tilde{c}_{\alpha\beta}$, which have been computed using DFPT, are also presented. These elastic constants can be converted to hypothetical equivalent bulk elastic constants by multiplying them by the corresponding out-of-plane lattice parameters and give values comparable to the bulk elastic constants reported in Table S1.

Afterwards, similarly to what has been done for example in Ref. [61], superlattices are built for each of the two 2D materials in play. Then, they are compared to each other for a given zigzag rotation angle θ_z between the layers [see Fig. 1(b)]. This angle is obtained by comparing zigzag directions in both phosphorene and graphene. Due to the symmetry of graphene and phosphorene primitive cells, θ_z take values between 0° and 30°. The reference ($\theta_z = 0°$) is taken as the configuration where the zigzag direction of phosphorene is aligned with the one of graphene. Note that, even in this case, graphene

TABLE I. Zigzag lattice parameter a, armchair lattice parameter b, layer thickness h, and planar elastic constants (per area unit) of phosphorene and graphene as predicted by PBE-D3. For comparison, we report the theoretical lattice parameters of Refs. [9] and [31].

	Phosphorene			Graphene	
	Lattice parameters (Å)				
	a^{P}	b^{P}	h^{P}	a^{C}	
PBE-D3	3.30	4.59	2.12	2.46	
PBE [9]	3.35	4.62			
optB88-vdW [31]	3.34	4.54			
	Elastic constants (J/m^2)				
	$\tilde{c}^{\text{P}}_{11}$	$\tilde{c}^{\text{P}}_{22}$	$\tilde{c}^{\text{P}}_{12}$	$\tilde{c}^{\text{C}}_{11}$	$\tilde{c}^{\text{C}}_{12}$
PBE-D3	103	23.0	17.3	356	63.4
		$\tilde{c}^{\text{P}}_{66}$			$\tilde{c}^{\text{C}}_{66}$
PBE-D3		23.2			145

and phosphorene lattices do not match, neither in terms of symmetries nor in terms of lattice parameters.

By stretching the phosphorene layer by a strain tensor $\underline{\underline{\epsilon}}$,[1] close to unity (deviations remain under 10%), one can construct a large set of commensurate structures [see Fig. 1(c)] and that for many different rotation angles. Afterwards, the structures that are equivalent by symmetry are discarded using PYMATGEN's geometry analyzer [62]. Finally, the structures that minimize the optimum function "strain × surface" are fed to the ABINIT code. Note that the strain can break the equivalence between zigzag directions of the graphene lattices. Accordingly, the primary zigzag vector $\vec{a}^{\,\mathrm{C}}$ is defined as the graphene zigzag vector whose angle is the smallest with respect to the phosphorene zigzag vector (unambiguously defined). The primary armchair vector $\vec{b}^{\mathrm{C}}$ is then defined as the graphene armchair vector that is the closest to the perpendicular to the primary zigzag vector. Moreover, the strain tensor used to make graphene and phosphorene lattices commensurate with each other might break the perpendicularity of armchair and zigzag vectors in each material and may induce a misalignment of crystalline directions of graphene and phosphorene. In order to take into account this effect, the deformation angles δ_i and armchair rotation angle θ_a are defined as follows:

$$\theta_a = \theta_z - (\delta_{\mathrm{phosphorene}} - \delta_{\mathrm{graphene}}) \approx \theta_z - 2\left(\bar{\epsilon}^{\mathrm{C}}_{\gamma} - \bar{\epsilon}^{\mathrm{P}}_{\gamma}\right), \quad (2)$$

where δ_i corresponds to the angle between the armchair and zigzag directions in the considered 2D lattice (graphene or phosphorene) within the vdW heterostructure, $\bar{\epsilon}^{\mathrm{P}}_{\gamma}$ and $\bar{\epsilon}^{\mathrm{C}}_{\gamma}$ are the (averaged) in-plane shear strains of phosphorene and graphene lattices compared to their free-standing counterparts, respectively.

It has to be reminded that the systems considered in this work are "bulk" graphene-phosphorene vdW heterostructures, obtained by stacking periodically both graphene and phosphorene layers [see Fig. 1(c)]. Still, in contrast to simple layered materials like graphite, not only a "translational" ordering is possible (AA, AB,...), but a "stacking" ordering as well, as illustrated for the latter case in Fig. 1(d). Different compositions of graphene and phosphorene layers in the vdW heterostructures are also considered. In the following, to differentiate these different structures, $\mathrm{G_iP_j}$ will denote each considered graphene-phosphorene vdW heterostructure, where i and j are, respectively, the number of consecutive graphene and phosphorene layers. Only periodic structures where at most three identical layers are nearest neighbors will be considered here, as illustrated in Fig. 1(f).

III. INTERLAYER ROTATION ANGLES AND STABILITY

In this section, the energy landscape of the graphene-phosphorene vdW heterostructures with respect to the rotation angles between the layers is investigated by *ab initio* means in order to pinpoint favorable alignments of the constituent layers. To do so, a small relevant set of commensurate phases was selected among the infinite number of structural configurations

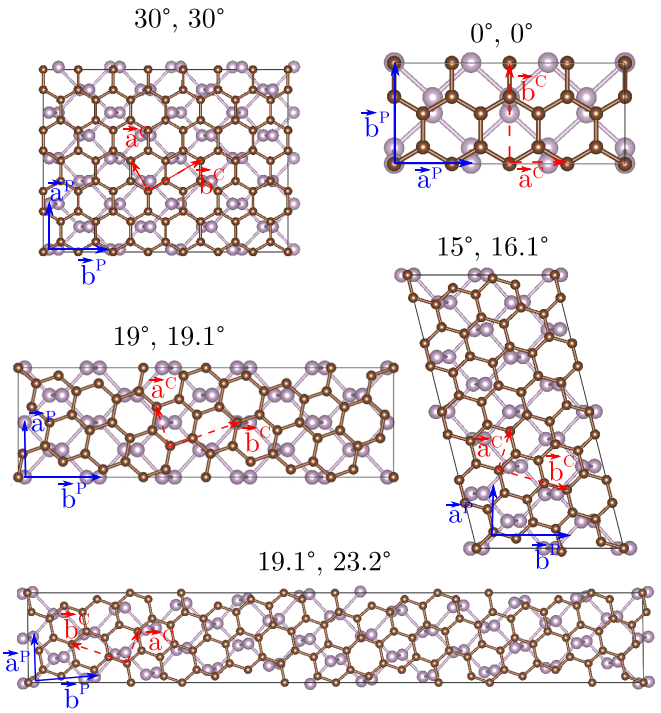

FIG. 2. The five commensurate structures investigated in this paper, characterized here by the zigzag (θ_z) and armchair (θ_a) rotation angles between the graphene and phosphorene layers. The primary zigzag ($\vec{a}^{\mathrm{C}}$) and armchair ($\vec{b}^{\mathrm{C}}$) vectors of graphene are represented in dashed red. Similarly, the primary zigzag ($\vec{a}^{\mathrm{P}}$) and armchair ($\vec{b}^{\mathrm{P}}$) vectors of phosphorene are shown in solid blue. The average strain tensors of graphene ($\underline{\bar{\epsilon}}^{C}$) and of phosphorene ($\underline{\bar{\epsilon}}^{P}$) are then defined based on their respective primary lattice vectors.

for the vdW heterostructures, considering the possible effective angles between the layers. Here, five different structures consisting of one graphene and one phosphorene layer periodically repeated out of plane ($\mathrm{G_1P_1}$) and with a limited number of atoms (<200) are investigated. These five constructed structures correspond to different zigzag and armchair rotation angles θ_z and θ_a, and a top view of their primitive cells is shown in Fig. 2. The numbers of repeated graphene or phosphorene lattice vectors [illustrated in Fig. 1(a)], used to build the heterostructure, are 2D vectors denoted, respectively, $\vec{n}^{\mathrm{C}}_{\alpha}$ and $\vec{n}^{\mathrm{P}}_{\alpha}$. The different atomic structures have been optimized in DFT; their characteristics, i.e., rotation angle θ_z and θ_a, number of atoms N_{at}, atomic fraction of phosphorus atoms x are presented in Table II, alongside with the average strain by primitive cell of phosphorene and graphene $\underline{\bar{\epsilon}}^{\mathrm{P}}$ and $\underline{\bar{\epsilon}}^{\mathrm{C}}$.

The first-principle calculations show that graphene distorts only weakly to accommodate to phosphorene while the latter takes most of the deformation, as expected when one refers to their respective planar elastic constants in Table I. Indeed, the in-plane phosphorene elastic constant along the armchair direction c^{P}_{22} is 25 times smaller than the in-plane graphene elastic constant c^{C}_{11}. For each of these commensurate structures, the strain remains sufficiently small, such that the change in the intralayer-neighbor distance in the vdW heterostructure (distance between neighbors belonging to the same layer), remains similar to the one of black phosphorus/graphite, as

[1]Due to the large ratio of elastic constants between graphite and black phosphorus (at least bigger than ten), we consider in first approximation that phosphorene takes all the deformation.

TABLE II. Characteristics and in-plane properties of the graphene-phosphorene vdW heterostructures (vdW-HS) studied in this paper. Each vdW-HS is characterized by its zigzag and armchair rotation angles θ_z and θ_a, its number of atoms N_{at}, and its fraction of phosphorus atom x. The in-plane properties reported here are the number of graphene and phosphorene primitive cells used along the heterostructure lattice vectors $\vec{n}_\alpha^{\,C}$ and $\vec{n}_\alpha^{\,P}$ to build the full structure and the averaged graphene and phosphorene strain tensors (in Voigt notation) $\underline{\underline{\bar{\epsilon}}}^{C}$ and $\underline{\underline{\bar{\epsilon}}}^{P}$.

	Characteristics				In-plane graphene properties					In-plane phosphorene properties				
vdW-HS	θ_z (°)	θ_a (°)	N_{at} (/)	x (/)	$\vec{n}_1^{\,C}(\vec{a}_1^{\,C},\vec{a}_2^{\,C})$ (/, /)	$\vec{n}_2^{\,C}(\vec{a}_1^{\,C},\vec{a}_2^{\,C})$ (/, /)	$\bar{\epsilon}_a^{C}$ (%)	$\bar{\epsilon}_b^{C}$ (%)	$\bar{\epsilon}_\gamma^{C}$ (%)	$\vec{n}_1^{\,P}(\vec{a}^{\,P},\vec{b}^{\,P})$ (/, /)	$\vec{n}_2^{\,P}(\vec{a}^{\,P},\vec{b}^{\,P})$ (/, /)	$\bar{\epsilon}_a^{P}$ (%)	$\bar{\epsilon}_b^{P}$ (%)	$\bar{\epsilon}_\gamma^{P}$ (%)
$G_1P_1(0°, 0°)$	0	0	28	0.43	(4,0)	(1,2)	0.1	0.2	0.0	(3,0)	(0,1)	−0.1	−6.8	0.0
$G_1P_1(15°, 16.1°)$	15	16.1	96	0.42	(3,−1)	(4,8)	−0.3	0.0	0.1	(0,2)	(5,1)	0.4	−3.3	−0.9
$G_1P_1(19°, 19.1°)$	19.0	19.1	96	0.42	(8,−2)	(2,3)	0.1	−0.2	0.1	(0,5)	(2,0)	−1.0	−1.8	0.0
$G_1P_1(19.1°, 23.2°)$	19.1	23.2	192	0.42	(16,−4)	(2,3)	−0.2	0.3	0.5	(1,10)	(2,0)	−1.0	−1.5	−3.1
$G_1P_1(30°, 30°)$	30	30	148	0.43	(7,0)	(0,3)	0.1	0.8	0.0	(0,4)	(4,0)	−2.1	−5.9	0.0
$G_1P_2(0°, 0°)$	0	0	40	0.60	(4,0)	(1,2)	0.1	0.2	0.0	(3,0)	(0,1)	−0.1	−6.8	0.0
$G_2P_1(0°, 0°)$	0	0	44	0.27	(4,0)	(1,2)	0.1	0.2	0.0	(3,0)	(0,1)	−0.1	−6.8	0.0
$G_2P_2(0°, 0°)$	0	0	56	0.43	(4,0)	(1,2)	0.1	0.2	0.0	(3,0)	(0,1)	−0.1	−6.8	0.0
$G_3P_3(0°, 0°)$	0	0	84	0.43	(4,0)	(1,2)	0.1	0.2	0.0	(3,0)	(0,1)	−0.1	−6.8	0.0

illustrated in Fig. S1. For some commensurate structures, the strain is not homogeneously shared between all the primitive cells of phosphorene, as illustrated in Fig. S1c, indicating local deformations. The average interlayer distance between graphene and phosphorene layers $\langle d_{\text{int}} \rangle$ is reported in Table III. The latter drastically varies depending on the effective angle but always lies in between the graphite (3.48 Å) and black phosphorus (3.19 Å) predicted interlayer distances. Some corrugations at the graphene-phosphorene interfaces are observed for specific effective angles and only for phosphorene (graphene stays flat). To quantify this effect, the standard deviation of the corrugation height is defined:

$$\sigma_d = \frac{1}{\sqrt{4N_{\text{P}}}}\left(\sqrt{\sum_{i\in \text{top}}\left(z_t^{\text{P}i} - \bar{z}_t^{\text{P}}\right)^2} + \sqrt{\sum_{i\in \text{bottom}}\left(z_b^{\text{P}i} - \bar{z}_b^{\text{P}}\right)^2}\right), \tag{3}$$

where $z_t^{\text{P}i}$ and $z_b^{\text{P}i}$ are the Cartesian coordinates in the out-plane direction of phosphorus atom i which belongs to the top and bottom planes of phosphorene, respectively; $\bar{z}_t^{\text{P}}$ and $\bar{z}_b^{\text{P}}$ are the average positions out of plane of the top and bottom layers of phosphorene; N_{P} is the number of phosphorus atoms in the heterostructure. This corrugation standard deviation always remains below 0.02 Å and is found to be negligible for the $\theta_z = \theta_a = 0°$ structure.

The comparison of the relative stability of these heterostructures can now be performed. However, the ratio between the number of carbon and phosphorus atoms is not identical in the different structures, and thus their total energies cannot be straightforwardly compared. The standard treatment for comparing materials with varying composition relies on the introduction of chemical potentials for each species, in the grand canonical formalism. In the present case, however, one can define as reference different reservoirs of carbon and phosphorus atoms: either the isolated monolayers (graphene and phosphorene), or bulk graphite and black phosphorus. Both will be considered, with different designation: "cohesive energy" and "mixing energy." Later, this analysis of stability will be refined by introducing two other concepts: the "stacking energy" and the "substitution energy."

So, first, let us define the cohesive energy per atom of the vdW heterostructure with respect to graphene and phosphorene:

$$E_{\text{coh}} = \frac{E_{\text{HS}}}{N_{\text{HS}}} - x\,\mu_{\text{P}} - (1-x)\,\mu_{\text{C}}, \tag{4}$$

where E_{HS} is the computed total energy of the vdW heterostructure, N_{HS} its number of atom per commensurate structure, x is the fraction of phosphorus atoms, $\mu_{\text{P}} = E_{\text{P}}/N_{\text{P}}$ the chemical potential of phosphorus computed in phosphorene, where E_{P} is the total energy of phosphorene and N_{P} its number of atoms per primitive cell. This cohesive energy expresses the gain in energy to form the vdW heterostructure compared to the isolated layers. It is reported in Table III. Note that this definition of cohesive energy for graphite and for black phosphorus is consistent with the one introduced in Sec. II and used in Table S1. From the negative values in this table, we can conclude that the condensation of phosphorene and graphene layers is always exothermic, thus spontaneous. However, it remains to determine which phase condenses preferentially with respect to the others, and in particular whether graphene-phosphorene heterostructures are stable with respect to graphite and black phosphorus.

Compared to isolated phases of graphite and black phosphorus, a given vdW heterostructure is more stable if its cohesive energy is smaller than a reference energy

$$E_{\text{ref}} = x\,E_{\text{coh}}^{\text{BP}} + (1-x)\,E_{\text{coh}}^{\text{Gr}}, \tag{5}$$

where $E_{\text{coh}}^{\text{BP}}$ and $E_{\text{coh}}^{\text{Gr}}$ are the cohesive energies of black phosphorus and graphite, respectively. To give an order of magnitude, the reference energy is −66.5 meV/atom for $x = 0.42$. The change of phosphorus fraction between the different heterostructures modifies this last value by less than 1 meV/atom.

This stability assessment, that differs from the one relative to isolated graphene and phosphorene, is facilitated by the use of the mixing energy instead of the cohesive energy. The

TABLE III. Out-of-plane properties of the graphene-phosphorene vdW heterostructures (vdW-HS) studied in this paper, i.e., average interlayer distance $\langle d_{\text{int}} \rangle$, the standard deviation of the phosphorene corrugation height σ_d, cohesive energy E_{coh}, mixing energy E_{mix}, stacking energy E_{stack}, and substitution energy E_{sub}.

vdW-HS	Out-of-plane properties					
	$\langle d_{\text{int}} \rangle$ (Å)	σ_d (Å)	E_{coh} (meV/atom)	E_{mix} (meV/atom)	E_{stack} (meV/atom)	E_{sub} (meV/atom)
$G_1P_1(0°, 0°)$	3.25	≈0	−62.8	4.4	−68.5	2.8
$G_1P_1(15°, 16.1°)$	3.33	0.005	−61.4	5.3	−62.5	4.8
$G_1P_1(19°, 19.1°)$	3.33	0.01	−61.5	5.2	−62.3	4.4
$G_1P_1(19.1°, 23.2°)$	3.31	0.02	−56.1	10.6	−62.3	4.8
$G_1P_1(30°, 30°)$	3.30	0.01	−55.1	12.3	−65.2	6.4
$G_1P_2(0°, 0°)$	3.23	≈0	−70.4	3.8	−78.9	1.5
$G_2P_1(0°, 0°)$	3.25	≈0	−56.7	3.8	−60.4	2.6
$G_2P_2(0°, 0°)$	3.26	≈0	−62.8	4.2	−68.8	2.5
$G_3P_3(0°, 0°)$	3.25	≈0	−63.5	3.4	−69.6	1.6

mixing energy expresses the gain (or loss) of energy to form the heterostructure compared to graphite and black phosphorus,

$$E_{\text{mix}} = E_{\text{coh}} - E_{\text{ref}} = \frac{E_{\text{HS}}}{N_{\text{HS}}} - x\,\mu_{\text{P}}^{\text{BP}} - (1-x)\,\mu_{\text{C}}^{\text{Gr}}, \quad (6)$$

where $\mu_{\text{P}}^{\text{BP}}$ and $\mu_{\text{C}}^{\text{Gr}}$ are the chemical potentials computed in black phosphorus and graphite, respectively. The difference between the cohesive energy and the mixing energy is simply the reference energy. If the mixing energy is smaller than 0, it is more energetically favorable to form the heterostructure than forming isolated bulk phases of graphite and black phosphorus. The mixing energies reported in Table III are always positive (endothermic), although their magnitudes are quite small so that entropy will probably be able to drive the mixing at room temperature depending on the synthesis process.

Although this definition of mixing energy allows one to study the stability of different commensurate structures with respect to another, it does not allow us to investigate directly how the energy varies with respect to the rotation angle between the layers. Indeed, a given commensurate structure may not be the global energy minimum for a given rotation angle between the layers. In this case, the study of the vdW-heterostructures stability based on a finite set of commensurate structures and as a function of the rotation angles is futile. In order to overcome this difficulty, one can first identify the real energy minimum of a given rotation angle, by removing the spurious elastic energy and interlayer energy, and then compare it to others in order to identify the most favorable angle. This first solution is investigated using the model presented in Sec. IV. From this model, one can extract the contributions that need to be added to the mixing energy in order to reach the ground state for a given rotation angle between the layers as discussed later. However, one can alternatively try to find a definition of energy that is less sensitive to the choice of the commensurate structures in use. Indeed, the relative energy of the different commensurate structures can be split in (1) their difference in elastic energies, needed to match their lattice vectors, and (2) their difference in interlayer energies (including van der Waals, but not only) at the commensurate lattice vectors. As for the previous analysis, one can take as reference either the monolayers or the bulk materials.

First, we define a stacking energy corresponding to the gain in energy obtained by taking as reference isolated graphene and phosphorene layers stretched to match the heterostructure lattice vectors:

$$E_{\text{stack}} = \frac{E_{\text{HS}}}{N_{\text{HS}}} - x\,\mu_{\text{P}}|_{\bar{\bar{\epsilon}}_{\text{HS}}^{\text{P}}} - (1-x)\,\mu_{\text{C}}|_{\bar{\bar{\epsilon}}_{\text{HS}}^{\text{C}}}. \quad (7)$$

In this last expression, $\mu_{\text{P}}|_{\bar{\bar{\epsilon}}_{\text{HS}}^{\text{P}}}$ and $\mu_{\text{C}}|_{\bar{\bar{\epsilon}}_{\text{HS}}^{\text{C}}}$ are the chemical potentials of phosphorus and carbon, respectively, computed at the corresponding phosphorene and graphene strained lattices in the vdW heterostructure $\bar{\bar{\epsilon}}_{\text{HS}}^{\text{P}}$ and $\bar{\bar{\epsilon}}_{\text{HS}}^{\text{C}}$. These strained lattices correspond to the ones obtained from the averaged strain tensors reported in Table II, and the internal degrees of freedom are optimized. Compared to the cohesive energy, the stacking energy is less sensitive to the change in intralayer energy due to the strains used to match graphene and phosphorene lattices, and allows the comparison of direct stacking.

Similarly to this stacking energy, which refers to the free-standing 2D materials, one can define the substitution energy which is based on the chemical potentials computed in the bulk:

$$E_{\text{sub}} = \frac{E_{\text{HS}}}{N_{\text{HS}}} - x\,\mu_{\text{P}}^{\text{BP}}\big|_{\bar{\bar{\epsilon}}_{\text{HS}}^{\text{P}}} - (1-x)\,\mu_{\text{C}}^{\text{Gr}}\big|_{\bar{\bar{\epsilon}}_{\text{HS}}^{\text{C}}}, \quad (8)$$

where $\mu_{\text{P}}^{\text{BP}}|_{\bar{\bar{\epsilon}}_{\text{HS}}^{\text{P}}}$ and $\mu_{\text{C}}^{\text{Gr}}|_{\bar{\bar{\epsilon}}_{\text{HS}}^{\text{C}}}$ are the chemical potentials of phosphorus/carbon computed in black phosphorus and graphite, respectively, and at the corresponding in-plane strain tensors in the vdW heterostructure. The interlayer distances between these strained graphene and phosphorene layers and the internal degrees of freedom are optimized. Although relatively simple, this substitution energy for a given rotation angle between the layers is found to be in good agreement with the results given by the model of Sec. IV. The variation of the substitution energy is only possible through the change of interlayer energies in the vdW heterostructure, graphite and black phosphorus, which are in principle all different, but are found to approximatively counterbalance each others. This definition of substitution energy is thus well suited in order to investigate the energy landscape as a function of the rotation angle between the layers and to the available literature.

These different definitions of energy and related chemical potentials are summarized and illustrated in Fig. 3, the

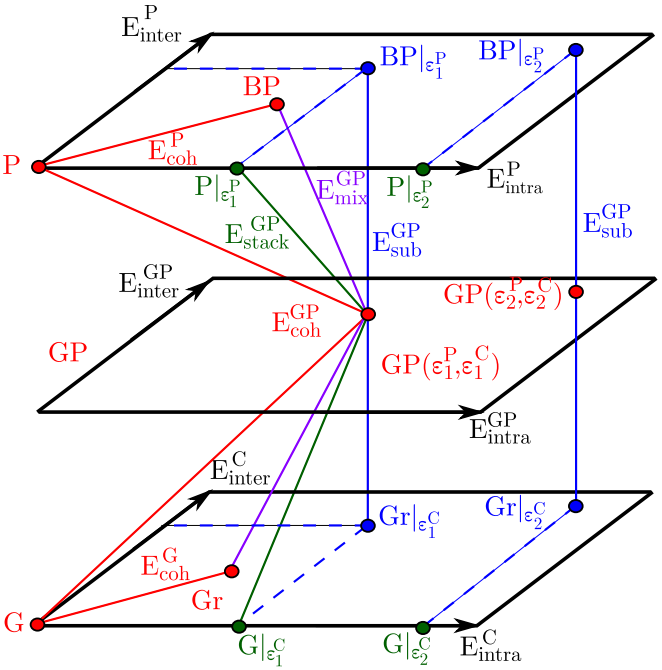

FIG. 3. Schematic representation of the different definitions of energies: cohesive, mixing, stacking, and substitution energies. The scheme is split into three planes, corresponding each to a different system (upper plane: black phosphorus, middle plane: graphene-phosphorene vdW heterostructure, bottom plane: graphite). For sake of clarity, the intralayer and interlayer energies of each system are the plane axes. G and P abbreviate graphene and phosphorene, respectively, Gr and BP their bulk counterparts (graphite and black phosphorus), while GP stands for the graphene-phosphorene vdW heterostructure. The cohesive energy E_{coh} and mixing energy E_{mix} are trivially defined by the scheme. The stacking energy E_{stack} is defined from the phosphorene and graphene geometries in the vdW heterostructure, themselves characterized by the average strain tensors $\bar{\bar{\epsilon}}^{\text{P}}$ and $\bar{\bar{\epsilon}}^{\text{C}}$ (the tensor and average notations are dismissed here for sake of clarity), respectively. Finally, the substitution energy E_{sub} is defined from the same strained phosphorene and graphene in-plane geometries, but now stacked in the optimal stacking sequence on top of each other (interlayer distance optimized). By construction, the intralayer energies computed in the vdW heterostructure and in strained graphite and black phosphorus cancel out. Only remains the difference between interlayer interactions. If neglected, the substitution energy is independent of the commensurate structure in use ($E_{\text{sub}}[\epsilon^{\text{P}}_1,\epsilon^{\text{C}}_1] = E_{\text{sub}}[\epsilon^{\text{P}}_2,\epsilon^{\text{C}}_2]$).

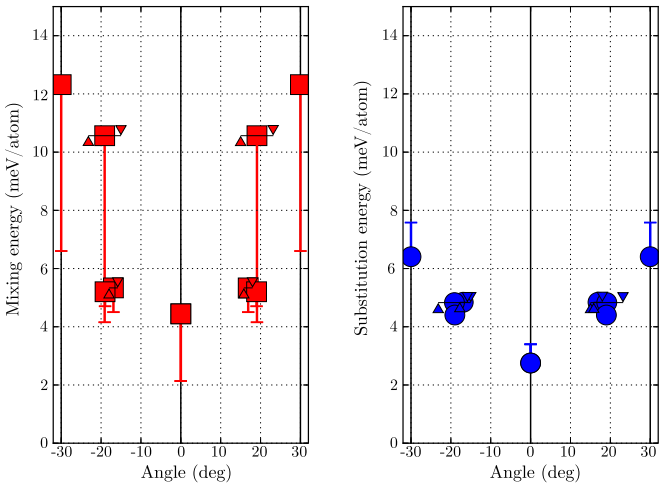

FIG. 4. (Left) Mixing energy E_{mix} and (right) substitution energy E_{sub} for the different G_iP_j vdW heterostructures as a function of the zigzag and armchair rotation angles θ_z and θ_a. The red square and blue circle symbols correspond to the mixing and substitution energies, respectively, and the angle intervals $[\theta_z,\theta_a]$ are delimited thanks to short horizontal lines with upward and downward arrows. Using the model presented in Sec. IV, the differences between a given commensurate structure and the estimated ground state for that specific rotation angle are shown using error bars for both mixing and substitution energies.

computed values for the different vdW heterostructures given in Table III, and the dependence of mixing and substitution energies with respect to the rotation angles shown in Fig. 4. Using the model presented in Sec. IV, the differences between a given commensurate structure and the estimated ground state for that specific rotation angle are shown using error bars, for both the mixing and substitution energies.

In terms of mixing energy, the most favorable structure corresponds to $G_1P_1(0^\circ, 0^\circ)$ which is surprisingly not the one that minimizes the sum of graphene and phosphorene strains (large compression of phosphorene armchair lattice) and that even when the spurious elastic and interlayer energies are removed. The spread in energy between all the investigated structures is about 8 meV/atom. Still, all these structures are quite far (>1 meV/atom) from their corresponding estimated ground states, with the notable exceptions of $G_1P_1(15^\circ, 16.1^\circ)$ and $G_1P_1(19^\circ, 19.1^\circ)$. On the contrary, the difference in terms of substitution energy between the studied structures and their corresponding estimated ground states (<1.2 meV/atom) is acceptable in view of the rotation angle energy landscape. Note that the estimated ground states obtained either through mixing or substitution energies are consistent with respect to one another. Based on our results, the substitution energy appears to be a smooth function of the rotation angle that admits one minimum at $\theta_z = \theta_a = 0^\circ$ (zigzag on zigzag and armchair on armchair). The computed spread in substitution energy is of approximatively 3.6 meV/atom, or 4.1 meV/atom using the estimated ground states. Still, based on the stacking energy, the possibility that armchair on zigzag ($\theta_z = \theta_a = 30^\circ$) cannot be excluded and could thus be a favorable alignment as well.

To the best of our knowledge, there have been no theoretical or experimental investigations on the energy landscape as a function of the rotation angle between the layers for graphene-phosphorene vdW heterostructures. Consequently our results can only be compared to the cases of other studied vdW heterostructures, which involve generally much stiffer materials than phosphorene (graphene, h-BN or transition-metal dichalcogenides), with the exception of silicene and germanene. Theoretical investigations of this rotation degree of freedom [15,30] have generally been performed using extremely large supercells, in which the layers kept their original lattice parameters, sometimes based on experimental observation of lattice matching. However, this situation should not be hypothesized *a priori* in *ab initio* calculations. It corresponds to artificially imposing a nonmodification of the

independent monolayer lattice parameters. However, for the sake of comparison, it will be assumed here that both their reported energy and our substitution energies can be directly compared.

First, similarly to what is found for graphene bilayers [21], graphene on h-BN [14,15], silicene on MoS_2 [18], germanene on MoS_2 [20], and MoS_2 on graphene [19] some rotation angles are found more favorable—the so-called magic angles. More specifically, the most stable configuration corresponds to the alignment of the crystalline directions (e.g., zigzag on zigzag) of the 2D materials in play in the vdW heterostructure, similarly to what is reported in Refs. [14,15,18–21], although not all of these heterostructures are reported as commensurate (MoS_2 on graphene, for example). In contrast, Constantinescu and Hine did not find theoretically any remarkably-favorable rotation angle between the layers in the case of $MoSe_2$ on MoS_2 [30]. Contrarily to what it first seems, we do not think their results go against the previously-mentioned observations. In fact, we suspect that the energy landscape with respect to rotation is flatter in the case of $MoSe_2$ on MoS_2 than in our case due to (a) large lattice mismatch and (b) large elastic constants for the two layers in play.

Finally, as the most favorable angular configuration has been identified for the graphene-phosphorene vdW heterostructure as 0°, one can now investigate the stability of these heterostructures as a function of the stacking composition fixing the rotation angles $\theta_z = \theta_a = 0°$ (G_1P_1, G_2P_1, G_1P_2, G_2P_2 and G_3P_3). During the relaxation, it is found for these vdW heterostructures that the most stable translational-stacking configuration is AB stacking for adjacent graphene layers[2] and for adjacent phosphorene layers.[3] A nonspecific translational vector is observed at the interface between graphene and phosphorene layers as shown in Fig. S2 for the G_1P_1 vdW heterostructure. The cohesive, mixing, stacking, and substitution energies of these structures are displayed in Table II. It is found that, by atom, all G_iP_j configurations are really close in terms of substitution energy (<1 meV/atom). This indicates that the formation of a graphene-phosphorene bulk vdW composite is not driven by enthalpy, which would lead to specific stacking arrangement like G_1P_1 but by entropy. Still, the synthesis process of the graphene-phosphorene bulk vdW composite could allow one to tune its stacking sequence by, for example, exfoliating and depositing the layers on top of each other one by one. The experimental stacking composition of vdW heterostructures is mostly limited by the exfoliation technique. If it produces few-layers thick graphene and phosphorene multilayers (between 5 and 10) then the vdW heterostructures would also be composed of graphene and phosphorene domains of the same thickness. This may reveal critical for specific applications, when the properties of interest, such as the cyclability in a sodium-ion battery [7], may depend strongly on this stacking composition. Finally, it is worth mentioning that the average interlayer distance between graphene and phosphorene layers does not vary significantly with respect to the stacking composition (∼3.25 Å) and lies in between the one of graphite and black phosphorus.

[2]Translation of a carbon-carbon distance in the armchair direction between two adjacent layers.

[3]Translation of a half zigzag lattice parameter in the zigzag direction between two adjacent layers.

IV. INTRALAYER DEFORMATION

The goal of the present section is to provide an approach to investigate the (eventual) averaged intralayer deformation of the different constituent layers in the graphene-phosphorene vdW heterostructures. Indeed, contrary to graphene, h-BN, or transition-metal dichalcogenides, phosphorene is soft in the armchair direction, indicating that it is easy to deform it in order, for example, to maximize its interlayer interactions. This effect should be relatively decorrelated to the question of phase coherency, as it is already observed in black phosphorus. In this material, all the constituent phosphorene layers match the others by symmetry, independently of the strains they undergo. Still, the armchair lattice parameter of phosphorene varies strongly going from the monolayer to the bulk (see Tables S1 and I) only due to the interlayer interactions. Similar effects are thus expected to appear in the graphene-phosphorene vdW heterostructures, although their amplitude has to be determined, which proves to be puzzling. Indeed, the approach followed in the previous section does not allow us to explore the intralayer-deformation degrees of freedom, since working with a given commensurate structure fixes approximatively the lattice parameters of phosphorene in order to accommodate to the ones of graphene. In consequence, the phosphorene-deformation energy map cannot be simply explored without considering different commensurate structures, some of them being extremely costly of presently available simulations. In addition, this intralayer deformation could still occur in the case of incommensurate vdW heterostructures, as reported in the case of germanene grown on MoS_2 [20].

In order to overcome this difficulty, a simple model is constructed based on the hypothesis [13–15] that the important terms that drive surface reconstruction, or intralayer deformation, are the interlayer (hereby only considering vdW as discussed latter) and intralayer (elastic) energies and that they can be decoupled. The general approach is presented here for two given 2D materials in which the crystalline directions are aligned, i.e., zigzag on zigzag and armchair on armchair. In this case, the use of the conventional cell of graphene defined by one zigzag unit vector and one armchair unit vector is more convenient for comparison with the primitive cell of phosphorene. The number of times these unit vectors for the layer i are repeated along the given axis α to form the heterostructure is denoted n_α^i, in contrast to the notation of Sec. II, where it was formally required to work with vectorial quantities. The model can be easily extended for any given rotation angle between the layers. This model is further verified on graphite and black phosphorus, before being applied to the case of graphene-phosphorene vdW heterostructure.

The sum of elastic and vdW energies, that determines entirely the deformation of the phosphorene and graphene layers, can be written as

$$\Delta E = E_{\text{elast}}\left(n_\alpha^{(1)}, n_\alpha^{(2)}\right) + E_{\text{vdW}}\left(n_\alpha^{(1)}, n_\alpha^{(2)}\right), \tag{9}$$

where $n_\alpha^{(1)}$ and $n_\alpha^{(2)}$ are the numbers of repeated primitive cells of the first and second 2D materials in the direction α used to build the heterostructure, respectively. For the

sake of simplicity, the effect of shear strains and internal relaxations originating from the counterbalance of vdW forces, interatomic force constants, and internal strain parameters [54] are neglected. Their supercell lattices match:

$$n_\alpha^{(1)} a_\alpha^{(1)} - n_\alpha^{(2)} a_\alpha^{(2)} = 0, \tag{10}$$

where a_α^{i} are the lattice parameters of the corresponding 2D materials. The residual strain, resulting from the lattice mismatch between the supercells, is equilibrated between the two layers such as the global surface tension vanishes:

$$\tilde{\sigma}_\beta = \sum_\beta n_\alpha^{(1)} \tilde{c}_{\alpha\beta}^{(1)} \epsilon_\alpha^{(1)} + \sum_\beta n_\alpha^{(2)} \tilde{c}_{\alpha\beta}^{(2)} \epsilon_\alpha^{(2)} = 0, \tag{11}$$

where $\tilde{c}_{\alpha\beta}^{(1)}$ and $\tilde{c}_{\alpha\beta}^{(2)}$ are the elastic constants of the two 2D materials per surface unit, $\epsilon_\alpha^{(1)}$ and $\epsilon_\alpha^{(2)}$ their strain by primitive cells. With the exception of an equivalent rescaling of the graphene and phosphorene superlattices, the strain is unambiguously defined by the numbers of repeated primitive cells. The total strains undergone by the layers are split equally between all its constituent unit cells. To this set of strains corresponds a certain elastic energy given by

$$E_{\mathrm{elast}} = \frac{A_0^{(1)}}{2} \sum_{\alpha,\beta} \tilde{c}_{\alpha\beta}^{(1)} \epsilon_\alpha^{(1)} \epsilon_\beta^{(1)} + \frac{A_0^{(2)}}{2} \sum_{\alpha,\beta} \tilde{c}_{\alpha\beta}^{(2)} \epsilon_\alpha^{(2)} \epsilon_\beta^{(2)}, \tag{12}$$

where $A_0^{(1)}$ and $A_0^{(2)}$ are the undeformed surfaces defined by the 2D lattices of the first and second 2D material, respectively. Afterwards, the vdW energy is itself estimated within the DFT-D3 method, that only requires the atomic positions and the exchange-correlation functional, based on the lattice-matched structure. The interlayer distance is fixed to the one of graphite and black phosphorus in the case of their respective analysis, and to the one of $G_1P_1(0^\circ, 0^\circ)$ in the case of the vdW heterostructure. The vdW energy is found nearly independent to the translation between the layers in the case of vdW heterostructure. In all the cases, the vdW energies of the relaxed isolated layers are subtracted to the computed vdW energy (per atom) in order to get only the "interlayer" vdW interactions:

$$E_{\mathrm{vdW}} \to E_{\mathrm{vdW}} - x \frac{E_{\mathrm{vdW}}^{\mathrm{P}}}{N_{\mathrm{P}}} - (1-x) \frac{E_{\mathrm{vdW}}^{\mathrm{C}}}{N_{\mathrm{C}}}, \tag{13}$$

where $E_{\mathrm{vdW}}^{\mathrm{P}}$ and $E_{\mathrm{vdW}}^{\mathrm{C}}$ are the vdW energies of undeformed phosphorene and graphene, respectively. Afterwards, the reference for the vdW energy is defined as the one in which the constituent layers are neither stretched nor compressed.

It is expected that the lattice parameters of the two 2D materials remain relatively similar (less than 10% at least) in the vdW heterostructure compared to the ones in their free-standing forms. In consequence, the ratio between the number of primitive cells of graphene and phosphorene in a given direction is chosen as close as the inverse ratio of their free-standing lattice parameters $a_{0,\beta}$,

$$\frac{n_\alpha^{(1)}}{n_\alpha^{(2)}} \approx \frac{a_{0,\alpha}^{(2)}}{a_{0,\alpha}^{(1)}}. \tag{14}$$

In practice, $n_1^{\mathrm{P}}/n_1^{\mathrm{C}}$ ratios range from 7/10 to 4/5 in the zigzag direction and $n_2^{\mathrm{P}}/n_2^{\mathrm{C}}$ ratios ranges from 9/10 to 1/1 in the armchair direction. Interestingly, taking an irrational number for this ratio corresponds in reality to investigate incommensurate superlattices of graphene and phosphorene.

Even with this model, scanning the entire configurational space in the case of the vdW heterostructure is computationally demanding. In consequence, the elastic energy is estimated for all the combination of superlattice vectors while the vdW energy only for specific points of the mesh. These points, expressed in terms of phosphorene strains, are shown in Fig. S3. It is found that the interlayer vdW energy in black phosphorus and in the vdW heterostructure shows on average a linear dependency with respect to the phosphorene deformation (both along the zigzag and armchair directions). Thus, this vdW energy can be interpolated with respect to the zigzag and armchair strains for the remaining superlattices of the graphene-phosphorene vdW heterostructures. Their energy landscape as a function of the phosphorene deformation is illustrated in Fig. S3. Hereafter, only the results for specific cuts in the strain planes, which correspond to the lines along which the vdW energy was estimated, will be shown.

The fact that both the elastic and interlayer vdW energies are varying continuously with strain for phosphorene has an important physical consequence. Indeed, it implies that even in the case of an incommensurate (incoherent) interface, phosphorene can still accommodate in average to graphene, that the effect can be quantified and non-negligible, as discussed later in this paper. This effect adds up to the possible local accommodation of phosphorene to graphene, that will determine the type of interfaces they form together (i.e., coherent, semicoherent, or incoherent). The Moiré interference pattern of graphene and phosphorene is relatively complex, as shown in Fig. S4, due to the lack of shared symmetries between these 2D materials and their large lattices mismatches. In addition, the Moiré period varies with the averaged strain undergone by the constituent layer (here, phosphorene) in agreement with what is observed experimentally for graphene grown on h-BN [12]. This makes the investigation of local accommodation and its impact on energetics incredibly challenging, and we prefer here to highlight already the large effect of a global accommodation of phosphorene to graphene.

The results of the present model are depicted in Fig. 5 for all the considered systems: On the left, the variation of the vdW and elastic energies are shown with respect to the zigzag lattice parameter of either graphene (in graphite) or phosphorene (in black phosphorus and in the vdW heterostructure), while on the right the same quantities are presented with respect to armchair lattice parameter. Note the change of energy scale between the different panels. The results for graphite are shown in the top panels [Fig. 5(a)], black phosphorus in the middle panels [Fig. 5(b)], and the vdW heterostructure in the bottom panels [Fig. 5(c)].

The change in vdW energy is rather linear with respect to the in-plane lattice parameter, being directly proportional to the density of atoms in the changed layer: the highest the density, the lowest the vdW energy. The gain in vdW energy by compressing graphene or phosphorene in the zigzag direction is nearly negligible when compared to the corresponding loss in elastic energy. In consequence, the relaxed zigzag lattice parameters of graphene and phosphorene in graphite, black phosphorus, and in the vdW heterostructure are close to the ones of the corresponding free-standing counterparts, in

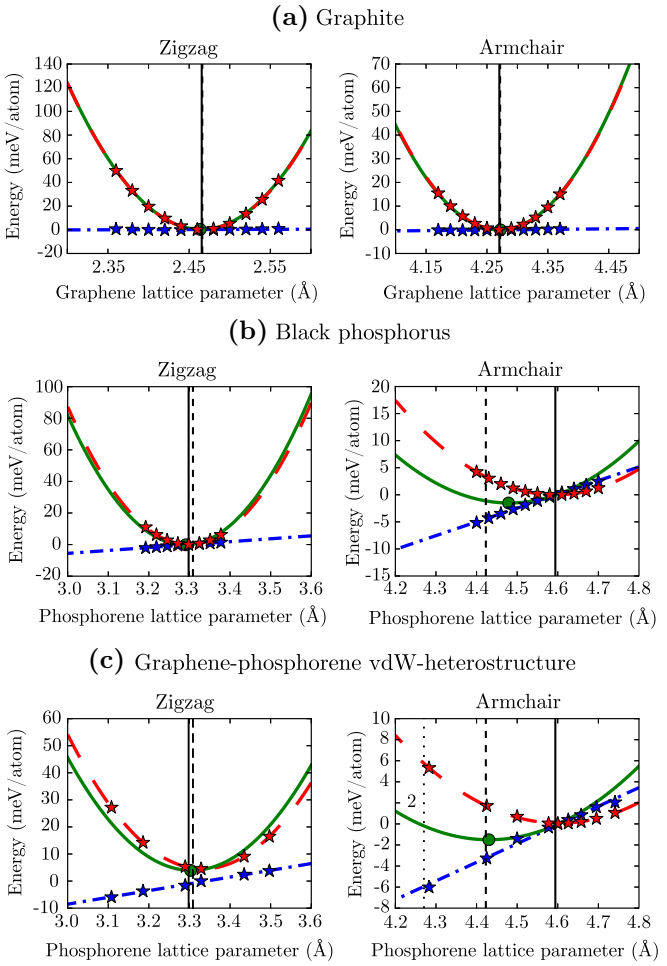

FIG. 5. Variation of (dashed red) elastic energy, (dotted blue) vdW energy, (solid green) energy sum as defined in Eq. (9) as a function of (left) zigzag lattice parameter and (right) armchair lattice parameter. The top panels correspond to the case of graphite, the middle panels to black phosphorus, while the bottom panels correspond to the case of the graphene-phosphorene vdW heterostructures. For comparison, in panel (a), the lattice parameters of graphene and graphite along the considered direction are displayed in solid black and in dotted black, respectively. In panel (b), the lattice parameters of phosphorene and black phosphorus along the considered direction are displayed in solid black and in dotted black, respectively. For the left panel (c), the zigzag lattice parameters of phosphorene and black phosphorus are displayed in solid black and in dotted black, respectively. For the right panel (c), the armchair lattice parameters of phosphorene and black phosphorus are displayed in solid black and in dotted black, respectively, while the armchair lattice parameter of graphene is displayed in dotted black. Stars correspond to the computed values, and circles correspond to the minima of the total energy.

agreement with what has been reported in Tables S1 and I. On the contrary, in the armchair direction, the gradient of vdW energy plays an important role for phosphorene, as it is of the same order of magnitude as the variation in elastic energy. Our computations show that, when they are stacked upon another, phosphorene layers will tend to contract in order to decrease their total energy, as observed previously in black phosphorus. With the simple model presented in this section, we are able to understand the origin of such phenomenon, albeit qualitatively. An accurate quantitative description requires the addition of the interlayer change in kinetic, Hartree, Ewald, (non)local pseudopotential, exchange-correlation and core pseudopotential energies with strains, which would be the topic of further work. Still, our model allows us to understand why the most favorable predicted structure exhibits a large armchair contraction of phosphorene.

In Fig. 5(c) are presented the results related to the graphene-phosphorene vdW heterostructure with respect to both zigzag and armchair directions. The change with graphene lattice parameters is not shown, because it is extremely similar to the graphite case, i.e., negligible. Similarly to black phosphorus, the zigzag parameter of phosphorene in the heterostructure is only weakly affected by the vdW interactions with the graphene layers. The armchair lattice parameter is on the contrary strongly modified by these interactions, and is predicted to contract more than in black phosphorus. This global ∼4% contraction is predicted independently of the nature of the interface, and thus it should even be present in the case of an incommensurate graphene-phosphorene vdW heterostructure. Still, this value remains mostly indicative, as our model does not include all the DFT ingredients as it normally should, but the functional and dispersion corrections have as well their own limited accuracies.[4] Furthermore, local accommodations can induce further global straining of phosphorene, up to a ∼7% compression on average for a pseudocoherent interface between graphene and phosphorene: the $G_1P_1(0°, 0°)$ studied in Sec. III. This commensurate structure consists of 3×1 phosphorene and 4×1 graphene conventional cells and has already been investigated in the literature [25,33,34] in the case of graphene-supported phosphorene. However, to the best of our knowledge, it has been done by fixing the lattice either to the ones of isolated phosphorene or to an arithmetic average of graphene and phosphorene lattice constants, without considering the differences in elastic constants between graphene and phosphorene, a hypothesis that is not valid according to our computations. Similar hypotheses are made in the case of h-BN/phosphorene vdW heterostructures [33,63,64], as graphene and h-BN lattice parameters only differ by ∼2%. We stress here is that it is expected that phosphorene will contract largely when stacked on graphene or h-BN. The magnitude of this effect remains in question, as well as the type of interface (coherent, semicoherent, or incoherent) that will be formed.

Still, several additional informations can be extracted from this model. First, and most importantly, as it is so soft in the armchair direction, phosphorene will tend to accommodate to any material it is in contact with, e.g., graphene, in order to maximize its vdW energy, and the effect can be quite important (∼4%). This indicates strong substrate effect on the structural properties of phosphorene, and by extension on its electronic properties, which are extremely sensitive to strain [65] (direct to indirect gap transition). This will be discussed in more detail in the next section. This effect may also explain why the positions of the Raman peaks of phosphorene monolayer

[4]PBE-D3 overestimates the experimental lattice parameter of black phosphorus by approximatively 1%, see Table S1.

and multilayers are experimentally reported to be close in frequency [66] (differences smaller than 5 cm^{-1} between phosphorene and black phosphorus Raman peaks), while one would expect the contrary when referring to the change of the armchair lattice parameter between phosphorene and black phosphorus and the influence of strain on the Raman peaks of phosphorene [67] (of the order of 30 cm^{-1} for the change of lattice parameter from monolayer to the bulk predicted, i.e., ∼4%). Indeed, if the substrate induces a contraction of the armchair lattice parameter of phosphorene to a value close to the one of black phosphorus, then one would expect relatively close Raman peak positions [66]. As it will be shown, the changes in electronic properties are also important, nearly turning the direct gap of phosphorene into an indirect one, and thus specific features should be observable in the resonant Raman spectroscopy [68] of supported/encapsulated phosphorene depending on the supporting or encapsulating material.

Second, based on our theoretical model, the energy difference between a given commensurate structure, characterized by its average strain tensors and rotation angles (see Table II), and the estimated ground state of our model can be estimated. To do so, the average strains of the constituent layers in the vdW heterostructure, as estimated based on our DFT computations, is fed in Eq. (9). Compared to the aligned case, the elastic energy includes additionally the contributions due to graphene and phosphorene shear strains. The change in vdW energy is itself estimated based on its linear interpolation along zigzag and armchair directions done previously in this section, neglecting thus its change with shear strain. The difference between this resulting (total) energy and the ground-state energy estimated by our model is then subtracted to the mixing energy computed using Eq. (6). Similar corrections are considered in the case of the substitution energy [Eq. (8)], but taking additionally into account of the change of elastic and vdW energies of graphite and black phosphorus with strain.

Finally, the validity of our model is investigated by comparing the elastic constants computed in DFPT for the vdW heterostructure and the theoretical model. Indeed, based on Eq. (12), the elastic constants of the heterostructure can be written as:

$$c^{\mathrm{HS}}_{\alpha\beta} = \frac{1}{d}\left(\tilde{c}^{\mathrm{C}}_{\alpha\beta}\left[1+\epsilon^{\mathrm{C}}_{\alpha}\right]\left[1+\epsilon^{\mathrm{C}}_{\beta}\right] + \tilde{c}^{\mathrm{P}}_{\alpha\beta}\left[1+\epsilon^{\mathrm{P}}_{\alpha}\right]\left[1+\epsilon^{\mathrm{P}}_{\beta}\right]\right), \quad (15)$$

where d is the lattice constant in the out-of-plane direction of the heterostructure. The elastic constants computed on the one hand by DFPT for $G_1P_1(0°, 0°, b_P = b_C)$ and on the other hand with Eq. (15) for $G_1P_1(0°, 0°, b_P = b_C)$ and for the most stable structure predicted by the model, denoted $G_1P_1(0°, 0°, b_P = 1.04 \times b_C)$, are reported in Table IV.

Overall, this simple model is able to reproduce within 10% the elastic constants of $G_1P_1(0°, 0°, b_P = b_C)$. When compared to the $G_1P_1(0°, 0°, b_P = 1.04 \times b_C)$ case, $G_1P_1(0°, 0°, b_P = b_C)$ has similar in-plane elastic constants. Note the slightly negative value for the c_{55} elastic constant, indicating a structural instability due to a shear deformation along the plane defined by the out-of-plane and armchair lattice vectors. The phosphorene layers sandwiching graphene layers would thus be translated compared to another, leading to a different translational stacking than the one considered in G_1P_1 up to now. This may also lead to variations in terms of mixing and substitution energy for the $G_1P_1(0°, 0°, b_P = b_C)$ heterostructure, which may lead to its stabilization when compared to the isolated phases of graphite and black phosphorus. Still, this instability is at the edge of DFT precision, and possibly our numerical accuracy, and its impact expected to be small; it will not thus be studied here and is left for future work.

TABLE IV. Elastic constants of the graphene-phosphorene vdW heterostructure $G_1P_1(0°, 0°)$ predicted either by PBE-D3 within the DFPT formalism [only for the commensurate where the armchair lattice parameters of graphene and phosphorene are matched $G_1P_1(0°, 0°, b_P = b_C)$], or using the model based on Eq. (9) and Eq. (15). In this last case, we give the predicted elastic constants for $G_1P_1(0°, 0°, b_P = b_C)$ and for the vdW heterostructure which corresponds to the energy minimum in Fig. 5, $G_1P_1(0°, 0°, b_P = 1.04 \times b_C)$.

	Elastic constants (GPa)								
	c_{11}	c_{22}	c_{12}	c_{33}	c_{13}	c_{32}	c_{44}	c_{55}	c_{66}
	$GP_1(0°, 0°, b_P = b_C)$								
PBE-D3	529	427	102	43	−7	−4	8	−1	208
Model	534	434	93						
	$GP_1(0°, 0°, b_P = 1.04 \times b_C)$								
Model	533	434	94						

V. ELECTRONIC PROPERTIES

Following our observations on the intralayer deformation of phosphorene in the graphene-phosphorene vdW heterostructures, the impact of such deformation on their electronic properties is investigated in the present section, and more specifically in the case of $G_1P_1(0°, 0°, b_P = b_C)$, taken as an approximation of the ground-state structure $G_1P_1(0°, 0°, b_P = 1.04 \times b_C)$ predicted by the theoretical model of Sec. IV. To do so, the electronic band structure of phosphorene is recalled in Fig. 6(b), alongside its corresponding Brillouin's zone [Fig. 6(a)]. On top, the electronic band structure of graphene is superimposed, in its conventional cell, supposing that its armchair reciprocal lattice vector[5] is matching its phosphorene counterpart, and that the zigzag reciprocal lattice vector is exactly 3/4 of its phosphorene counterpart. The Fermi levels of graphene and phosphorene have been aligned. Although fictional—obviously graphene and phosphorene lattices do not match, thus their reciprocal lattices do not match neither—this approach allows us to see where band crossings could potentially occur. Graphene is a zero-gap semiconductor, while phosphorene is a real semiconductor, with a nearly-direct gap at Γ of 0.84 eV predicted by PBE-D3. This value compares relatively well with the 1 eV obtained with PBE [9] or with the 0.89 eV computed with PBE corrected by Grimme's DFT-D2 [60]. However, it differs significantly from the experimental values reported up to now (between 1.4 and 2 eV [10]),

[5]The reciprocal lattice vector parallel to the armchair crystalline direction of phosphorene.

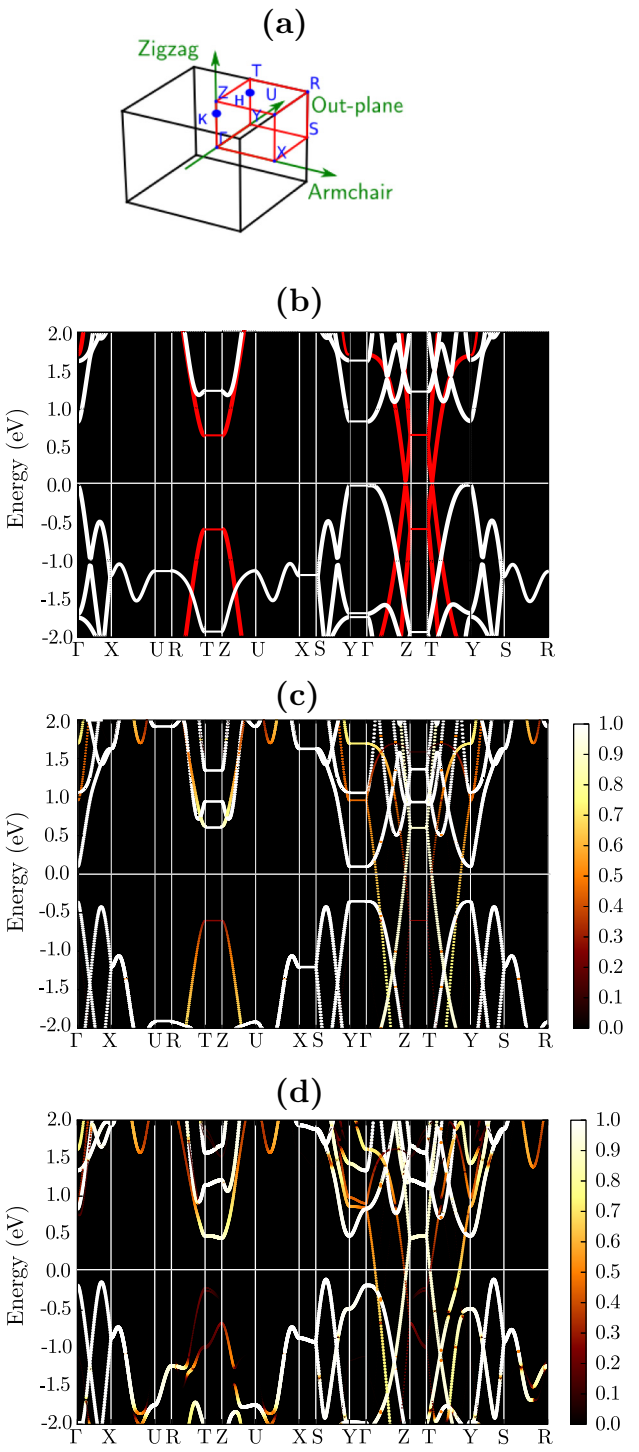

FIG. 6. Electronic band structures, unfolded on the Brillouin zone of phosphorene shown in (a), of (b) phosphorene (in white) and graphene (in red) monolayers superposed on top of each other, supposing that the graphene and phosphorene armchair lattices match and that the graphene zigzag lattice parameter is exactly 3/4 of its phosphorene counterpart. (b) Graphene and phosphorene strained such as the in-plane crystalline structure corresponds to the $G_1P_1(0°, 0°, b_P = b_C)$'s one. The layers are spaced by a 15-Å-thick vacuum layer to avoid in that case the interactions between the layers. (c) $G_1P_1(0°, 0°, b_P = b_C)$ graphene-phosphorene vdW heterostructure. The weight associated with the unfolding technique is given by the color bar and the marker size.

due, mainly, to the well-known underestimation of the gap in DFT [24]. Note that, close to the Fermi level, the bands of phosphorene and graphene do not cross each other, except along the R-T, Z-U, Y-Z, and T-Y lines. For the sake of comparison, we recall that graphite is a semimetal [69] and that black phosphorus is reported experimentally as a direct band gap semiconductor with a gap of ∼0.261 eV at 40 K [70]. Similarly to what is reported for example in Ref. [71], but with different dispersion corrections for the long-range e^--e^- correlation, our calculations predict black phosphorus to be metallic. In order to recover the correct electronic character of this material, beyond-DFT techniques (like G_0W_0) should be used [71].

Before discussing the electronic band structure of $G_1P_1(0°, 0°, b_P = b_C)$, one has to remind that the electronic properties of phosphorene are quite sensitive to strain, as reported for example in Ref. [65]. In order to de-correlate its effects from the one arising from the interactions with graphene (hybridization), we show the electronic band structure of graphene and phosphorene in Fig. 6(c) using the $G_1P_1(0°, 0°, b_P = b_C)$ in-plane geometry, but separating the layers by a 15-Å-thick vacuum layer such as the (electronic) interactions between the layers can be neglected. They are unfolded on the primitive cell of phosphorene using FOLD2BLOCH [72] as available in the ABINIT software. Note that the strain in the armchair direction of phosphorene (∼7%) can lead to important changes in the electronic band structures of the constituent layer. Notably, the second maximum in the valence band of phosphorene along the Γ-X high symmetry line is shifted upwards, and the minimum of the conduction band in phosphorene is strongly shifted downwards, shrinking its electronic gap by ∼0.35 eV, which is consistent with the observations in Ref. [65]. Graphene is only weakly affected by strain.

The electronic properties of the $G_1P_1(0°, 0°, b_P = b_C)$ structure, including thus now the interlayer interactions, is shown in Fig. 6(d). Compared to the previous case, where only the effects of strains were considered, several additional changes are noticeable. First, at the crossing of graphene and phosphorene bands in the lattice-matched case, avoided crossings can be observed in the electronic band structure of the vdW heterostructure, except along Γ-Z where the linear band of graphene crosses a band of phosphorene without being affected. We suppose in that case that the states are simply orthogonal to another. Second, the strain effect on the conduction band minimum of phosphorene is counterbalanced by the interaction with graphene, leading to a comparable direct electronic transition at Γ for phosphorene free standing or in the vdW heterostructure. This effect can announce a quantum confinement in the monolayer that disappears moving to the bulk graphene-phosphorene vdW heterostructure. Third, the band offset is quite small (<0.1 eV), indicating no important charge transfer between graphene and phosphorene layers. Fourth, large modifications of the band structures are observed out of plane, where lifts of degeneracy of the graphene and phosphorene electronic states are observed. The $G_1P_1(0°, 0°, b_P = b_C)$ vdW heterostructure is semimetallic, similarly to graphite. The first electronic transition between phosphorene states is found be indirect.

In consequence, the intrinsic electronic properties of phosphorene can be tuned by the environment (substrate or other),

not only by state-hybridization or dielectric screening, but also by vdW-induced strain as discussed in this paper. This finding may reveal itself to be critical for electronic applications, where it has been proposed to encapsulate phosphorene in h-BN to avoid its oxidation [31,60,73] without altering its electronic band structure. While the effect of state-hybridization [31] and dielectric screening [60] have already been investigated, the effect of vdW-induced strain should also play an important role, and should be investigated in more details for the h-BN/phosphorene/h-BN vdW heterostructure. Depending on the supporting or encapsulating material, it may even be possible to close the gap of phosphorene using such vdW-induced strain, although the strain required may be too important (contraction $>12\%$, according to Ref. [65]) to be achievable by vdW interactions only.

VI. CONCLUSION

In the present paper, the properties of bulk graphene-phosphorene vdW heterostructures have been investigated. First, their stability has been analyzed as a function of the rotation angle between the layers for different definition of chemical potentials and as a function of the stacking composition, thus finding that the most stable configuration corresponds to the alignment of graphene and phosphorene crystalline directions. A new concept of substitution energy is proposed to investigate this specific degree of freedom. The accommodation of phosphorene to graphene in the vdW heterostructure is then examined, notably in the armchair direction. To do so, a model based on the elastic and interlayer vdW energies is constructed, explaining the contraction of phosphorene armchair lattice parameter from the monolayer to the bulk (black phosphorus). In the graphene-phosphorene vdW heterostructures, it is found that phosphorene contracts as well in order to maximize its vdW interactions with graphene, leading to strong structural and electronic modifications. This effect is identified as independent of the nature of the interfaces (coherent, semicoherent, or incoherent). This leads to the conclusion that, in average, phosphorene will always compress quite importantly compared to its free-standing form in order to maximize its interactions with any material it is in contact with, even if they are bound only by weak dispersive forces. The present model can be easily transferred to study interfaces based on other 2D materials, like blue phosphorus [74], arsenene [75] or antimonene [76], for which it has yet to be determined if any lattice accommodation could occur. We suspect that the magnitude of the deformation will mostly depend on the softness of the materials in play (related to their elastic constants), but this will be the topic of other works. In parallel, the present model could be further refined in order to include the effects of local accommodations that may allow us to predict the formation of semicoherent or incoherent interfaces.

In consequence, this work calls into questions the role of the substrate on the intrinsic properties of phosphorene; such a role has to the best of our knowledge always been neglected up to now and thus may be re-investigated. More specifically, the impact of encapsulation of phosphorene between h-BN layers may lead to either undesired changes in the intrinsic electronic properties of phosphorene (direct to indirect gap transition) or on contrary positive changes, like an increase of the electronic mobility as observed for example in graphene encapsulated between h-BN layers [77]. We also mention the possibility of substrate-controlled stresstronic in phosphorene, where the gap could be tuned only based on the substrate. In parallel, the investigation of the sodiated phases of these graphene-phosphorene vdW heterostructures may allow us to understand better why their performance as anode in sodium-ion batteries are improved comparatively to black phosphorus or graphite [7].

ACKNOWLEDGMENTS

The authors acknowledge technical help from J.-M. Beuken and M. Giantomassi and scientific discussions with S. M.-M. Dubois and D. Di Stefano. This work has been supported by the FRS-FNRS through a FRIA Grant (B.V.T.) and two research projects (Nos. T.1077.15 & T.0051.18); the Communauté française de Belgique through the BATTAB project (ARC 14/19-057) and the *"3D nanoarchitecturing of 2D crystals"* project (ARC 16/21-077); the Région Wallone through the BATWAL project (No. 1318146); the European Union's Horizon 2020 research and innovation program (No. 696656). Computational resources have been provided by the supercomputing facilities of the Université catholique de Louvain (CISM/UCL) and the Consortium des Equipements de Calcul Intensif en Fédération Wallonie Bruxelles (CECI) funded by the Fonds de la Recherche Scientifique de Belgique (FRS-FNRS) under convention 2.5020.11. The present research benefited from computational resources made available on the Tier-1 supercomputer of the Fédération Wallonie-Bruxelles, infrastructure funded by the Walloon Region under the Grant agreement No. 1117545.

[1] K. S. Novoselov, A. Mishchenko, A. Carvalho, and A. H. Castro Neto, Science **353**, aac9439 (2016).

[2] A. K. Geim and I. V. Grigorieva, Nature (London) **499**, 419 (2013).

[3] L. M. Woods, D. A. R. Dalvit, A. Tkatchenko, P. Rodriguez-Lopez, A. W. Rodriguez, and R. Podgornik, Rev. Mod. Phys. **88**, 045003 (2016).

[4] K. Zhang, T. Zhang, G. Cheng, T. Li, S. Wang, W. Wei, X. Zhou, W. Yu, Y. Sun, P. Wang *et al.*, ACS Nano **10**, 3852 (2016).

[5] J. S. Ross, P. Rivera, J. Schaibley, E. Lee-Wong, H. Yu, T. Taniguchi, K. Watanabe, J. Yan, D. Mandrus, D. Cobden *et al.*, Nano Lett. **17**, 638 (2017).

[6] S. Latini, K. T. Winther, T. Olsen, and K. S. Thygesen, Nano Lett. **17**, 938 (2017).

[7] J. Sun, H.-W. Lee, M. Pasta, H. Yuan, G. Zheng, Y. Sun, Y. Li, and Y. Cui, Nat. Nano. **10**, 980 (2015).

[8] G.-C. Guo, D. Wang, X.-L. Wei, Q. Zhang, H. Liu, W.-M. Lau, and L.-M. Liu, J. Phys. Chem. Lett. **6**, 5002 (2015).

[9] H. Liu, A. T. Neal, Z. Zhu, Z. Luo, X. Xu, D. Tománek, and P. D. Ye, ACS Nano **8**, 4033 (2014).

[10] A. Castellanos-Gomez, J. Phys. Chem. Lett. **6**, 4280 (2015).

[11] D. A. Porter, K. E. Easterling, and M. Y. Sherif, *Phase Transformations in Metals and Alloys* (CRC Press, Boca Raton, 2009).

[12] A. Davies, J. D. Albar, A. Summerfield, J. C. Thomas, T. S. Cheng, V. V. Korolkov, E. Stapleton, J. Wrigley, N. L. Goodey, C. J. Mellor *et al.*, Nano Lett. **18**, 498 (2018).

[13] C. Woods, L. Britnell, A. Eckmann, R. Ma, J. Lu, H. Guo, X. Lin, G. Yu, Y. Cao, R. Gorbachev *et al.*, Nat. Phys. **10**, 451 (2014).

[14] D. Wang, G. Chen, C. Li, M. Cheng, W. Yang, S. Wu, G. Xie, J. Zhang, J. Zhao, X. Lu *et al.*, Phys. Rev. Lett. **116**, 126101 (2016).

[15] C. R. Woods, F. Withers, M. J. Zhu, Y. Cao, G. Yu, A. Kozikov, M. Ben Shalom, S. V. Morozov, M. M. van Wijk, A. Fasolino *et al.*, Nat. Commun. **7**, 10800 (2016).

[16] G. Argentero, A. Mittelberger, M. Reza Ahmadpour Monazam, Y. Cao, T. J. Pennycook, C. Mangler, C. Kramberger, J. Kotakoski, A. K. Geim, and J. C. Meyer, Nano Lett. **17**, 1409 (2017).

[17] N. R. Wilson, P. V. Nguyen, K. Seyler, P. Rivera, A. J. Marsden, Z. P. L. Laker, G. C. Constantinescu, V. Kandyba, A. Barinov, N. D. M. Hine *et al.*, Sci. Adv. **3**, e1601832 (2017).

[18] D. Chiappe, E. Scalise, E. Cinquanta, C. Grazianetti, B. van den Broek, M. Fanciulli, M. Houssa, and A. Molle, Adv. Mater. **26**, 2096 (2014).

[19] X. Liu, I. Balla, H. Bergeron, G. P. Campbell, M. J. Bedzyk, and M. C. Hersam, ACS Nano **10**, 1067 (2016).

[20] L. Zhang, P. Bampoulis, A. N. Rudenko, Q. Yao, A. van Houselt, B. Poelsema, M. I. Katsnelson, and H. J. W. Zandvliet, Phys. Rev. Lett. **116**, 256804 (2016).

[21] E. Koren, I. Leven, E. Lörtscher, A. Knoll, O. Hod, and U. Duerig, Nat. Nanotechnol. **11**, 752 (2016).

[22] J. Kang, J. Li, S.-S. Li, J.-B. Xia, and L.-W. Wang, Nano Lett. **13**, 5485 (2013).

[23] D. Pierucci, H. Henck, J. Avila, A. Balan, C. H. Naylor, G. Patriarche, Y. J. Dappe, M. G. Silly, F. Sirotti, A. T. C. Johnson *et al.*, Nano Lett. **16**, 4054 (2016).

[24] R. Martin, *Electronic Structure, Basic Theory and Practical Methods* (Cambridge University Press, Cambridge, 2004).

[25] J. E. Padilha, A. Fazzio, and A. J. R. da Silva, Phys. Rev. Lett. **114**, 066803 (2015).

[26] W. Hu, Z. Li, and J. Yang, J. Chem. Phys. **139**, 154704 (2013).

[27] W. Hu, T. Wang, and J. Yang, J. Mater. Chem. C **3**, 4756 (2015).

[28] N. Hine, P. Haynes, A. Mostofi, C.-K. Skylaris, and M. Payne, Comput. Phys. Commun. **180**, 1041 (2009).

[29] R. A. Bell, S. M.-M. Dubois, M. C. Payne, and A. A. Mostofi, Comput. Phys. Commun. **193**, 78 (2015).

[30] G. C. Constantinescu and N. D. M. Hine, Phys. Rev. B **91**, 195416 (2015).

[31] G. C. Constantinescu and N. D. M. Hine, Nano Lett. **16**, 2586 (2016).

[32] G. J. Slotman, M. M. van Wijk, P.-L. Zhao, A. Fasolino, M. I. Katsnelson, and S. Yuan, Phys. Rev. Lett. **115**, 186801 (2015).

[33] Y. Cai, G. Zhang, and Y.-W. Zhang, J. Phys. Chem. C **119**, 13929 (2015).

[34] X.-R. Hu, J.-M. Zheng, and Z.-Y. Ren, Front. Phys. **13**, 137302 (2017).

[35] S. Grimme, J. Anthony, S. Ehrlich, and H. Krieg, J. Chem. Phys. **132**, 154104 (2010).

[36] See Supplemental Material at http://link.aps.org/supplemental/10.1103/PhysRevMaterials.2.074001 for additional information on graphite and black phosphorus (lattice parameters, elastic energy, etc.) and additional figures related to the question of lattice conformation, translational degree of freedom, and of Moiré interference pattern.

[37] X. Gonze, G.-M. Rignanese, M. Verstraete, J.-M. Beuken, Y. Pouillon, R. Caracas, F. Jollet, M. Torrent, G. Zerah, M. Mikami *et al.*, Z. Kristallogr. **220**, 558 (2009).

[38] X. Gonze, B. Amadon, P.-M. Anglade, J.-M. Beuken, F. Bottin, P. Boulanger, F. Bruneval, D. Caliste, R. Caracas, M. Côté *et al.*, Comput. Phys. Commun. **180**, 2582 (2009).

[39] X. Gonze, F. Jollet, F. A. Araujo, D. Adams, B. Amadon, T. Applencourt, C. Audouze, J.-M. Beuken, J. Bieder, A. Bokhanchuk *et al.*, Comput. Phys. Commun. **205**, 106 (2016).

[40] M. Fuchs and M. Scheffler, Comput. Phys. Commun. **119**, 67 (1999).

[41] B. Van Troeye, M. Torrent, and X. Gonze, Phys. Rev. B **93**, 144304 (2016).

[42] D. R. Hamann, Phys. Rev. B **88**, 085117 (2013).

[43] M. J. van Setten, M. Giantomassi, E. Bousquet, M. J. Verstraete, D. R. Hamann, X. Gonze, and G.-M. Rignanese, Comput. Phys. Commun. **226**, 39 (2018).

[44] H. J. Monkhorst and J. D. Pack, Phys. Rev. B **13**, 5188 (1976).

[45] M. Methfessel and A. T. Paxton, Phys. Rev. B **40**, 3616 (1989).

[46] L. Cartz, S. R. Srinivasa, R. J. Riedner, J. D. Jorgensen, and T. G. Worlton, J. Chem. Phys. **71**, 1718 (1979).

[47] Y. Baskin and L. Meyer, Phys. Rev. **100**, 544 (1955).

[48] R. Zacharia, H. Ulbricht, and T. Hertel, Phys. Rev. B **69**, 155406 (2004).

[49] Y. Kôzuki, Y. Hanayama, M. Kimura, T. Nishitake, and S. Endo, J. Phys. Soc. Jpn. **60**, 1612 (1991).

[50] S. Appalakondaiah, G. Vaitheeswaran, S. Lebègue, N. E. Christensen, and A. Svane, Phys. Rev. B **86**, 035105 (2012).

[51] T. Bučko, S. Lebègue, J. Hafner, and J. G. Ángyán, Phys. Rev. B **87**, 064110 (2013).

[52] L. Shulenburger, A. Baczewski, Z. Zhu, J. Guan, and D. Tománek, Nano Lett. **15**, 8170 (2015).

[53] G. Savini, Y. Dappe, S. Öberg, J.-C. Charlier, M. Katsnelson, and A. Fasolino, Carbon **49**, 62 (2011).

[54] D. R. Hamann, K. M. Rabe, and D. Vanderbilt, Phys. Rev. B **72**, 033102 (2005).

[55] X. Wu, D. Vanderbilt, and D. R. Hamann, Phys. Rev. B **72**, 035105 (2005).

[56] D. R. Hamann, X. Wu, K. M. Rabe, and D. Vanderbilt, Phys. Rev. B **71**, 035117 (2005).

[57] B. Van Troeye, M. J. van Setten, M. Giantomassi, M. Torrent, G.-M. Rignanese, and X. Gonze, Phys. Rev. B **95**, 024112 (2017).

[58] A. Bosak, M. Krisch, M. Mohr, J. Maultzsch, and C. Thomsen, Phys. Rev. B **75**, 153408 (2007).

[59] M. Yoshizawa, I. Shirotani, and T. Fujimura, J. Phys. Soc. Jpn. **55**, 1196 (1986).

[60] D. Y. Qiu, F. H. da Jornada, and S. G. Louie, Nano Lett. **17**, 4706 (2017).

[61] D. S. Koda, F. Bechstedt, M. Marques, and L. K. Teles, J. Phys. Chem. C **120**, 10895 (2016).

[62] S. P. Ong, W. D. Richards, A. Jain, G. Hautier, M. Kocher, S. Cholia, D. Gunter, V. L. Chevrier, K. A. Persson, and G. Ceder, Comput. Mater. Sci. **68**, 314 (2013).

[63] T. Hu and J. Hong, ACS Appl. Mater. Interfaces **7**, 23489 (2015).
[64] L. E. Marsoner Steinkasserer, S. Suhr, and B. Paulus, Phys. Rev. B **94**, 125444 (2016).
[65] X. Peng, Q. Wei, and A. Copple, Phys. Rev. B **90**, 085402 (2014).
[66] A.-L. Phaneuf-L'Heureux, A. Favron, J.-F. Germain, P. Lavoie, P. Desjardins, R. Leonelli, R. Martel, and S. Francoeur, Nano Lett. **16**, 7761 (2016).
[67] R. Fei and L. Yang, Appl. Phys. Lett. **105**, 083120 (2014).
[68] E. del Corro, A. Botello-Méndez, Y. Gillet, A. L. Elias, H. Terrones, S. Feng, C. Fantini, D. Rhodes, N. Pradhan, L. Balicas *et al.*, Nano Lett. **16**, 2363 (2016).
[69] M. Terrones, A. R. Botello-Méndez, J. Campos-Delgado, F. López-Urías, Y. I. Vega-Cantú, F. J. Rodríguez-Macías, A. L. Elías, E. Muñoz-Sandoval, A. G. Cano-Márquez, J.-C. Charlier *et al.*, Nano Today **5**, 351 (2010).
[70] N. Ehlen, B. V. Senkovskiy, A. V. Fedorov, A. Perucchi, P. Di Pietro, A. Sanna, G. Profeta, L. Petaccia, and A. Grüneis, Phys. Rev. B **94**, 245410 (2016).
[71] A. N. Rudenko and M. I. Katsnelson, Phys. Rev. B **89**, 201408 (2014).
[72] O. Rubel, A. Bokhanchuk, S. J. Ahmed, and E. Assmann, Phys. Rev. B **90**, 115202 (2014).
[73] A. Favron, E. Gaufrès, F. Fossard, A.-L. Phaneuf-L'Heureux, N. Y.-W. Tang, P. L. Lévesque, A. Loiseau, R. Leonelli, S. Francoeur, and R. Martel, Nat. Mater. **14**, 826 (2015).
[74] Z. Zhu and D. Tománek, Phys. Rev. Lett. **112**, 176802 (2014).
[75] S. Zhang, Y. Zhong, L. Yafei, C. Zhongfang, and H. Zeng, Angew. Chem. Int. Ed. **54**, 3112 (2015).
[76] M. Fortin-Deschênes, O. Waller, T. O. Menteş, A. Locatelli, S. Mukherjee, F. Genuzio, P. L. Levesque, A. Hébert, R. Martel, and O. Moutanabbir, Nano Lett. **17**, 4970 (2017).
[77] C. R. Dean, A. F. Young, I. Meric, C. Lee, L. Wang, S. Sorgenfrei, K. Watanabe, T. Taniguchi, P. Kim, K. L. Shepard *et al.*, Nat. Nanotech. **5**, 722 (2010).